

Synthesis of chitosan-stabilised iron and nickel nanoparticles and the application in the reductive degradation of nimesulide

Andressa Aparecida Gonçalves¹, Annelise França Araújo¹, Manoel José Mendes Pires², Rodrigo Moreira Verly¹, Débora Vilela Franco², Leonardo Morais da Silva¹⁺

¹ Federal University of Vales do Jequitinhonha e Mucuri (UFVJM), Department of Chemistry, 5000 MGT 367 Hwy, km 583, 39100-000 Diamantina, Minas Gerais, Brazil

² Federal University of Vales do Jequitinhonha e Mucuri (UFVJM), Institute of Science and Technology - Faculty of Chemical Engineering, 5000 MGT 367 Hwy, km 583, 39100-000 Diamantina, Minas Gerais, Brazil

+ Corresponding author: Leonardo Morais da Silva, phone: +55 38 3532 6000, e-mail address: lsilvamorais@hotmail.com

ARTICLE INFO

Article history:

Received: January 21, 2018

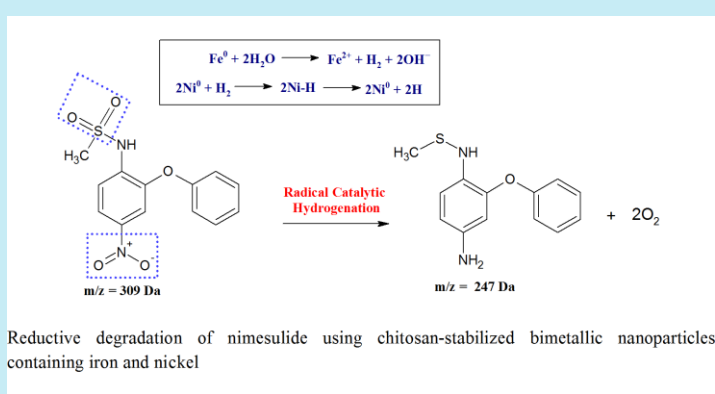
Accepted: May 9, 2018

Published: May 29, 2018

Keywords:

1. iron-nickel nanoparticles
2. emerging pollutants
3. stabilisation of nanoparticles
4. chitosan

ABSTRACT: Chitosan (CHI)-stabilised Ni-Fe bimetallic nanoparticles (bNP/CHI) were synthesised varying the content of nickel and denoted as 2-bNP/CHI, 17-bNP/CHI, and 27-bNP/CHI. The nanoparticles were characterised using several techniques and used in the removal of nimesulide. XRD and Mössbauer analyses confirmed the formation of an amorphous structure containing Fe⁰ and Fe₂O₃ while the FT-IR analysis confirmed the presence of chitosan in the nanoparticles. A very high removal of nimesulide was obtained after only 15 min of treatment with the 17-bNP/CHI system. The by-product obtained after the reductive treatment was identified using the chromatography analysis coupled to the mass spectrometry technique.



1. Introduction

Several organic substances used by the modern society are important pollutants which cause deleterious effects on the environment. In addition, several organic substances are classified as “emerging contaminants” and their occurrence in the environment is caused by the anthropic activities. Several studies have demonstrated the presence of different organic pollutants in rivers and wastewaters (e.g., drugs, pesticides, herbicides, hormones, etc.)¹⁻³.

The evaluation of the toxicological impacts on the environment of these classes of pollutants is not a facile task. Despite the fact that the pollution

burden is commonly found at low levels in the environment (e.g., in water bodies, in parts per billion or parts per trillion)¹⁻³, it is verified the simultaneous occurrence of several different anthropic substances for a given contaminated sample. Therefore, the complications arising from the combined toxicological effects comprise an environmental concern of extreme relevance. In addition, it is a fact that the emerging pollutants are not efficiently removed from contaminated waters and effluents using the traditional technologies based on physical and biological processes³.

From these considerations, the use of more efficient water and wastewater alternative treatment technologies is desirable to ensure that

the emerging contaminants can be effectively removed from the environment^{2, 3}. In principle, these contaminants can be removed using advanced reductive and/or oxidative chemical processes, which can permit the conversion of the toxic dissolved organic matter into less harmful substances⁴⁻⁶.

Regarding the occurrence of drugs in the environment, it was verified that the drug nimesulide (NMS) can be considered an emerging contaminant since its occurrence was already verified in different samples^{2, 3}. For instance, Papageorgiou *et al.*³ verified a high concentration of nimesulide in contaminated waters.

Nimesulide is a nitroaromatic substance/compound (e.g., NAC) widely used by the population due to its strong anti-inflammatory properties. In fact, nimesulide commonly exhibits better results for patients in comparison to other similar drugs (e.g., ibuprofen and diclofenac)⁷. The molecular structure of nimesulide (C₁₃H₁₂N₂O₅S) is shown in Figure 1. As can be seen, the molecular structure is characterised by an aromatic ring containing the phenyl and nitrophenyl groups interconnected to the other aromatic ring by an oxygen atom⁸.

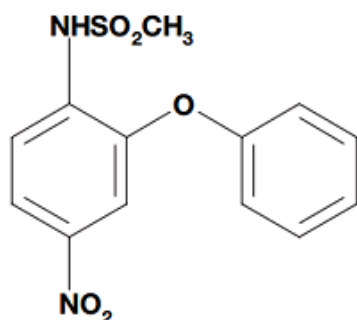


Figure 1. Chemical structure of nimesulide (NMS).

It is important to emphasise that the major deleterious effects on the environment caused by NACs are due to the nitroaromatic moiety present in these substances⁹⁻¹⁰. It is worth mentioning that NACs and the organochlorine substances are well-known contaminants that can be found in the environment. Fortunately, the negative impacts on the environment caused by NACs can be circumvented by removal of the functional nitro group in a redox reaction involving the use of different iron-containing particles (e.g., microparticles or nanoparticles). In this case, the parental substance (e.g., nimesulide) can be converted into less harmful substances (by-

products) that are naturally degraded in the environment⁹⁻¹⁰.

The modification of the zero-valent iron (ZVIn) system with incorporation of other metal can result in modifications in the reductive properties of the metallic system for heterogeneous redox reactions, as is the case of the reductive degradation of NACs. In fact, the use of a dissimilar metal, such as cobalt, nickel, and palladium, in conjunction with iron can permit to synthesise bimetallic systems highly active for the reductive degradation of different organic pollutants⁴⁻⁶. This type of bimetallic nanoparticle system (e.g., bNPs) was used with success in the reductive degradation of several organics¹⁰⁻¹³.

The magnetic properties of ZVIn and Fe-based bNPs cause the phenomenon of agglomeration, which in turn decrease the performance of the redox process (heterogeneous reaction) for the degradation of different organic pollutants. Thus, to avoid this undesirable phenomenon, these ferromagnetic nanoparticles are commonly stabilised/encapsulated using carboxymethyl cellulose (CMC) or chitosan (CHI). In addition, some studies reported the stabilisation of ferromagnetic nanoparticles by means of supporting them on silica microparticles^{11-12, 14-16}. It is worth mentioning that CHI is an important polymeric material used in the field of environmental nanotechnology due its interesting properties such as good biodegradability, biocompatibility, and low immunogenicity^{17, 18}.

The aims of the present work are: (i) the fabrication and characterisation of bimetallic nanoparticles composed of Fe and Ni stabilised with chitosan (CHI), denoted as bNP/CHI, and (ii) the study of the removal/transformation of nimesulide (NMS) in contaminated water during the redox reaction with the bNP/CHI system. The by-product obtained after the reductive treatment was identified using the chromatography analysis coupled to the mass spectrometry technique. A high degree of dispersibility was verified for the stabilised nanoparticles. As a result, a rapid removal of nimesulide was obtained using the bNP/CHI system.

2. Materials and methods

2.1 Materials

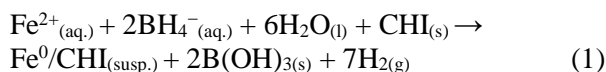
All chemicals used in this work (e.g., nimesulide, chitosan, FeSO₄·7H₂O, C₂H₄O₂, C₃H₆O, C₂H₅OH, NaBH₄, Ni(NO₃)₂·6H₂O, NaOH,

C₂H₃N, CH₃OH, and C₂HF₃O₂) were “Purum p.a.” products purchased from Sigma–Aldrich, Synth, and Fluka. High-quality chitosan from Sigma–Aldrich (product reference: C3646-100G) obtained from shrimp shells (*Pandalus borealis*) with a deacetylation degree $\geq 75\%$ was used throughout in this work.

Solutions were prepared using ultra-pure water obtained from a PURELAB (Brazil) purification system (model Classic Di-MK2).

2.2 Synthesis of the bNP/CHI system containing Ni and Fe

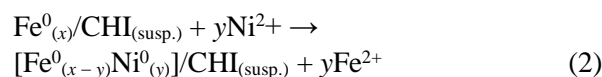
Firstly, the suspension containing the chitosan-stabilized zero-valent iron nanoparticles (Fe⁰/CHI_(susp.)) denoted as ZVIn/CHI_(susp.) was synthesised through chemical reduction of the Fe²⁺ ions using borohydride. In this case, 0.1 g of CHI_(s) was dissolved in 30 mL of a 5 % (v/v) acetic acid solution, while 2.0 g of FeSO₄·7H₂O was dissolved in 40 mL of water. These two solutions were mixed in an Erlenmeyer flask (e.g., reaction flask) resulting in a total volume of 70 mL. The mixture was agitated (250 rpm and 30 min) using an orbital shaker (IKA, model KS 260). After that, the pH was adjusted to 6.8 with the addition of some drops of a NaOH solution (5.0 M). After the previous immersion of the reaction flask in an ultrasonic bath (5 min), the reduction of Fe²⁺ was carried out by dropwise addition in the reaction flask of 6.90 mL of a NaBH₄ solution (2.3 M) under strong agitation (250 rpm and 5 min). The reduction of iron ions (Fe²⁺) resulted in the hydrogen evolution and a black suspension composed of the stabilised nanoparticles (Fe⁰/CHI_(susp.)) was obtained as represented by Equation 1:



In comparison with the non-stabilised Fe⁰-nanoparticles, it was verified that the use of CHI indeed increased the dispersibility of the Fe⁰-nanoparticles resulting in a stable black suspension (e.g., Fe⁰/CHI_(susp.)) that is not prone to agglomeration^{11, 18}.

In the second step of the synthesis, the suspension containing the stabilised bimetallic nanoparticles (Fe⁰–Ni⁰/CHI_(susp.), denoted as bNP/CHI_(susp.)) was obtained from the as-prepared Fe⁰/CHI_(susp.) nanoparticles through chemical

reduction of the Ni²⁺ ions. In this case, the chitosan-stabilised bimetallic nanoparticles containing Ni⁰ and Fe⁰ was obtained by adding 0.2615, 0.5230, and 1.046 g of Ni(NO₃)₂·6H₂O in the suspensions already containing the Fe⁰/CHI_(susp.) nanoparticles (250 rpm and 20 min). Therefore, the nominal (theoretical) Ni:Fe molar ratios considered in the present work were 0.125:1.0, 0.25:1.0, and 0.5:1.0, respectively. Each flask containing the as-prepared nickel solution (Ni²⁺_(aq.)) was covered using Parafilm®. In all cases, these flasks were immersed in an ultrasonic bath for 5 min. The suspension containing the stabilised nanoparticles was filtered (0.45- μm pore size) using a vacuum. Afterward, the suspension was rinsed using ethanol and acetone. As a result, the previously stabilised iron nanoparticles (Fe⁰/CHI_(susp.)) were partially covered with nickel as described by Equation 2:



As indicated in Equation 2, a fraction of the less noble metal (Fe) present in the Fe⁰/CHI_(susp.) nanoparticles was oxidized (Fe⁰ \rightarrow Fe²⁺_(aq.) + 2e⁻) in the presence of the Ni²⁺ ions with the concomitant reduction of the latter (Ni²⁺_(aq.) + 2e⁻ \rightarrow Ni⁰).

The energy dispersive X-ray spectrometry (EDS) technique was used to determine the real composition of the freshly prepared bimetallic nanoparticles (e.g., expressed in weight percentage, wt.%). It was obtained the following Ni:Fe weight ratios: 0.02:0.98, 0.17:0.83, and 0.27:0.73 (see further discussion). The nanoparticles were described as 2-bNP/CHI_(susp.), 17-bNP/CHI_(susp.), and 27-bNP/CHI_(susp.), respectively. The non-stabilised Ni–Fe bimetallic nanoparticles described as “bNP” were prepared using the aforementioned method in the absence of CHI.

2.3 Physicochemical characterisation of the bNP/CHI system

The composition of the nanoparticles was determined using the EDS technique (Oxford Instruments) with the aid of a scanning electron microscope from TESCAN. High-resolution images were obtained using a transmission electron microscope from FEI Tecnai (G2-20 SuperTwin at 200 kV). The structural analysis of the

nanoparticles was accomplished with the XRD technique (XRD-6000 diffractometer from Shimadzu) using standard conditions (Cu–K α radiation: $\lambda = 0.15406$ nm, 40 kV, 30 mA, and $0.2^\circ \text{min}^{-1}$). Fourier transform infrared (FT-IR) analyses were accomplished using a spectrometer from Varian (model 640-IR FT-IR). All samples were prepared using the standard KBr pellet method. ^{57}Fe Mössbauer analyses were conducted at 24°C under constant acceleration mode. The spectrometer was composed of Wissel and EG&G-Ortec modules using a $^{57}\text{Co}/\text{Rh}$ radiation source. The calibration procedure was done using a standard $\alpha\text{-Fe}$ foil. BET and BJH methods were used for evaluation of the specific surface area (SSA) ($\text{m}^2 \text{g}^{-1}$) and the pore size distribution (PSD), respectively. Experiments were carried out using a Quantachrome equipment (Autosorb-1).

2.4 Degradation of NMS with the bNP/CHI system

The degradation/transformation of nimesulide with the bNP/CHI_(susp.) system in water phase was accomplished at $24 \pm 3^\circ \text{C}$. The reactor flask (Erlenmeyer, $V = 100$ mL) was closed with Parafilm[®] to minimise the undesirable reaction (oxidation) of the as-prepared nanoparticles with the oxygen present in the air. The reaction medium (e.g., NMS and the nanoparticle suspension) was strongly agitated at different agitation frequencies using a model KS 260 orbital shaker from IKA.

The degradation of NMS (conditions: $[\text{NMS}]_0 = 40 \text{ mg L}^{-1}$ and $f = 250 \text{ rpm}$) with the bNP/CHI_(susp.) system was firstly accomplished as a function of the Ni⁰-percentage. Afterward, the particular composition of the bNP/CHI_(susp.) system that exhibited the best performance for the reductive degradation of NMS was used in the additional studies carried out as a function of the NMS and bNP/CHI_(susp.) concentrations. The agitation frequency was also varied in these studies (e.g., 0, 100, and 250 rpm). It is worth mentioning that no further changes were verified in the rate of the degradation process for agitation frequencies higher than 250 rpm.

For each experimental run, a new nimesulide solution ($V = 100$ mL and pH 11.7) was used for the reaction with the as-prepared bNP/CHI_(susp.) nanoparticles. Aliquots ($V = 5$ mL) were obtained at regular intervals of the reaction and then filtered ($0.45\text{-}\mu\text{m}$ pore size) for further chemical analyses.

2.5 Characterisation of the NMS solutions treated with the bNP/CHI_(susp.) system

All samples were analysed using the UV-Vis technique (Cary 50 from Varian). In addition, further experiments were conducted using the reverse-phase high-performance liquid chromatography (RP-HPLC) technique following the method reported in the literature¹⁹. A chromatograph from Varian (Pro Star 315) using an UV-detector was used throughout. Experimental conditions: $V = 20 \mu\text{L}$; $\lambda = 393 \text{ nm}$; $Q = 0.8 \text{ mL min}^{-1}$; C_{18} column (Nucleosil-Nucleodur: particle size = $3 \mu\text{m}$, $l = 125 \text{ mm}$, and $\varnothing = 4.6 \text{ mm}$). The isocratic elution was accomplished using a solution composed of acetonitrile/0.8% TFA and water/0.1% TFA (60:40 (v/v)).

2.6 Identification of the by-product formed after the reductive degradation of nimesulide

The by-product formed after the degradation/transformation of nimesulide during the redox reaction with the bNP/CHI_(susp.) system was obtained at an elution time of 5.3 min. This by-product was identified with the liquid chromatography-electrospray ionization-mass spectrometry (LC-ESI-MS) technique using a model LCMS-2020 system from SHIMADZU.

3. Results and discussion

3.1 Composition of the bimetallic system and the reductive degradation of nimesulide

The influence of nickel present in the bimetallic system (bNP/CHI_(susp.)) on the reductive degradation/transformation of nimesulide was investigated with the aid of the UV-Vis technique. Figure 2 shows the degradation of nimesulide as a function of the composition (e.g., nickel content) of the bimetallic system stabilised with chitosan.

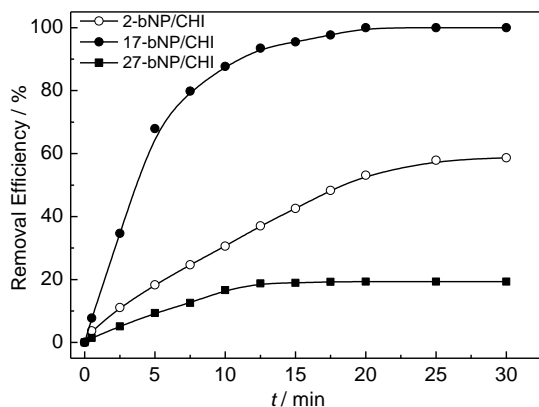


Figure 2. Dependence of the removal of NMS as a function of the nanoparticle composition. Conditions: $[NMS]_0 = 40 \text{ mg L}^{-1}$; $[bNP/CHI]_0 = 0.8 \text{ g L}^{-1}$; $f = 250 \text{ rpm}$; $T = 24 \pm 3 \text{ }^\circ\text{C}$.

As can be seen, removal efficiencies of 58 %, 100 %, and 20 % were achieved after 30 min of the redox reaction using the 2-bNP/CHI_(susp.), 17-bNP/CHI_(susp.), and 27-bNP/CHI_(susp.) systems, respectively. In addition, the degradation of nimesulide obeys a pseudo first-order kinetic model ($r^2 > 0.996$). In this sense, according to the experimental findings shown in Figure 2, the apparent rate constant (k_{ap}) depends on the Ni⁰-content with a maximum of 0.214 min^{-1} (17-bNP/CHI_(susp.)). Accordingly, k_{ap} -values of 0.0289 and 0.0177 min^{-1} were obtained for the 2-bNP/CHI_(susp.) and 27-bNP/CHI_(susp.) systems, respectively. According to the literature^{5, 20}, a possible explanation for this behaviour is a decrease in the surface concentration of the redox sites containing Fe⁰ promoted by a surface excess of the metallic centres containing the Ni⁰ species.

The best catalyst for the degradation of nimesulide was the 17-bNP/CHI_(susp.) system due to a trade-off between the surface concentrations of the active surface sites containing Fe⁰ (less noble metal) and the catalyst (e.g., Ni⁰), which in turn promotes the hydrogenation of NMS (see further discussion). Therefore, the 17-bNP/CHI_(susp.) system was then characterised with different ex-situ techniques (e.g., EDS, XRD, TEM, BET, FT-IR, and Mössbauer). In addition, this system was used on the degradation/conversion of nimesulide under different experimental conditions.

3.2 The composition of the nanoparticles and the degradation of nimesulide

The degradation of nimesulide as a function of the type of nanomaterial is shown in Figure 3.

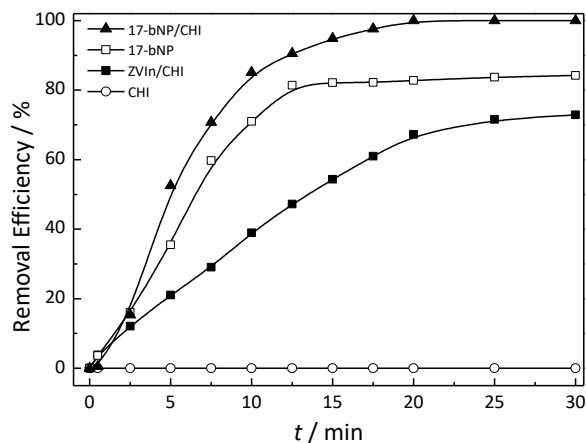


Figure 3. Influence of the composition of nanomaterial and chitosan on the removal of NMS. Conditions: $[NMS]_0 = 40 \text{ mg L}^{-1}$; $[\text{nanomaterial}]_0 = 0.8 \text{ g L}^{-1}$; $f = 250 \text{ rpm}$; $T = 24 \pm 3 \text{ }^\circ\text{C}$.

Figure 3 clearly shows that the degradation/removal of nimesulide depends on the composition of the nanomaterial. As can be seen, the best findings were obtained with the 17-bNP/CHI system. Removal percentages of 72 %, 84 %, and 100 % were obtained for nimesulide using the ZVIn/CHI, 17-bNP (e.g., non-stabilised), and 17-bNP/CHI systems, respectively. As expected, there was no removal of NMS using only the stabilising agent (CHI_(s)).

According to these results, a high dispersability of the stabilised nanoparticles in the aqueous medium has promoted the formation of a high active surface area for the redox reaction thus leading to an accentuated degradation rate of nimesulide. Also, due to its catalytic properties for the hydrogenation reaction²¹⁻²³, the Ni⁰-particles promoted the occurrence of the reductive degradation reaction (see further discussion). As can be seen, the other nanomaterials were less effective for the degradation of nimesulide. In principle, this behaviour can be correlated with the formation of a passive oxide layer which partially hinders the electron transfer in the active surface sites^{22, 23}. In addition, in this case, the formation of the H[•]-radicals is not catalysed causing a decrease in the rate for the overall redox reaction involving NMS.

3.3 The influence of the hydrodynamic conditions on the degradation reaction

The degradation rate of nimesulide can be affected by the hydrodynamic conditions (e.g., agitation frequency) since the redox reaction involving the Fe^0 -centres is a heterogeneous process with a possible influence of the mass-transport of the active species. In this sense, Figure 4 shows the influence of the agitation frequency on the degradation/removal of nimesulide using the bNP/CHI system.

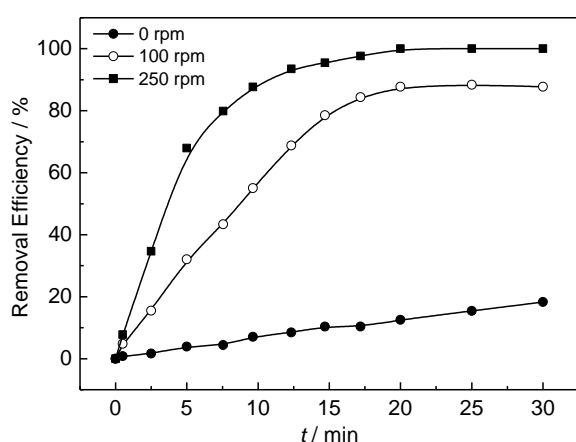


Figure 4. Influence of the agitation frequency (f) on the removal efficiency. Conditions: $[\text{NMS}]_0 = 40 \text{ mg L}^{-1}$; $[\text{17-bNP/CHI}]_0 = 0.8 \text{ g L}^{-1}$; $T = 24 \pm 3 \text{ }^\circ\text{C}$.

As seen, the removal of NMS depends on the hydrodynamic conditions as a consequence of the influence of mass-transport on the overall redox kinetics. It was verified a complete removal (100 %) of nimesulide after 20 min of reaction for an agitation frequency of 250 rpm. On the contrary, in the case of the other hydrodynamic conditions the removal was less than 83 %. Similar results were previously reported²⁴. The removal of NMS was not affected by agitation frequencies higher than 250 rpm. Therefore, it is assumed under this condition that the removal of nimesulide is under kinetic control and, therefore, the mass-transport no longer affects the heterogeneous redox reaction. All further studies in the present work were conducted at 250 rpm.

3.4 Physicochemical characterisation of the 17-bNP/CHI_(susp.) system

Figure 5 shows the TEM images obtained for the 17-bNP/CHI_(susp.) system.

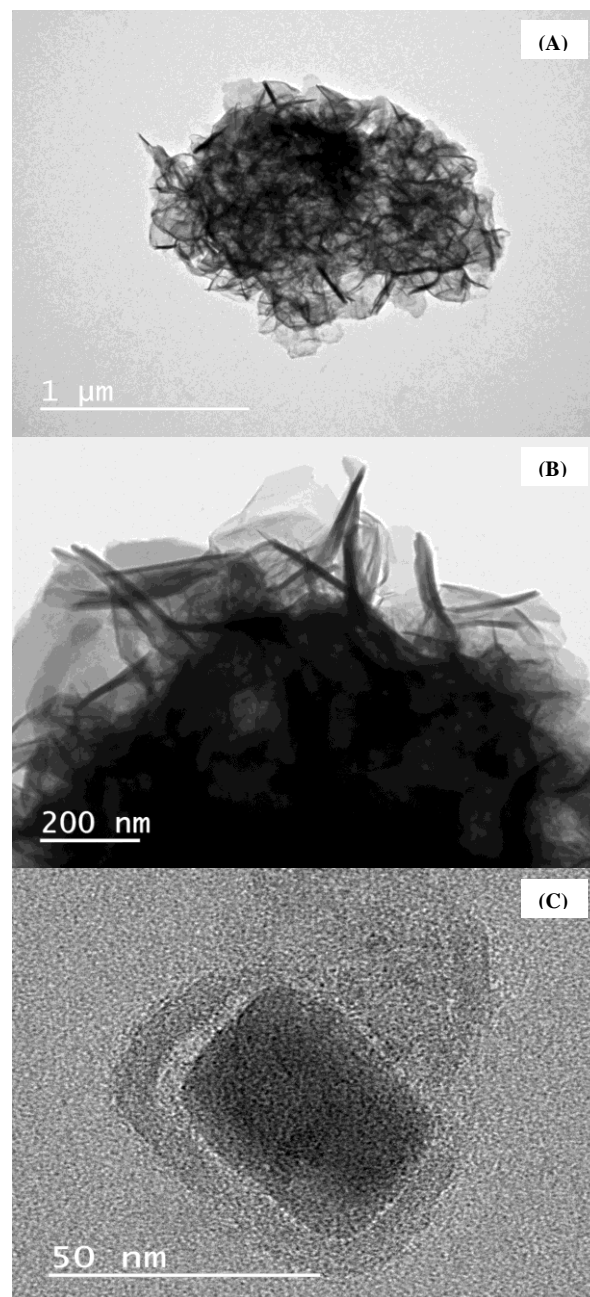


Figure 5. TEM images obtained for 17-bNP/CHI.

As can be seen, the individual clusters composed of bimetallic nanoparticles stabilised with chitosan (17-bNP/CHI_(susp.)) exhibit a rectangular morphology (Figure 5C) with a size of $\approx 50 \text{ nm}$. These findings are in agreement with the literature¹¹. In addition, according to the literature²², the bimetallic nanoparticles can be partially covered with a passive layer (e.g., Fe_3O_4 and/or Fe_2O_3) since the freshly synthesised

nanoparticles were in contact with the atmospheric air.

The EDS technique was used to obtain the composition of the metallic nanoparticles

expressed in weight percentage (wt.%) (see the Table 1).

Table 1. Elemental composition of the different nanoparticle systems expressed in wt.%

Element	ZVIn/CHI	17-bNP	2-bNP/CHI	17-bNP/CHI	27-bNP/CHI
C	20.7	-	26.2	22.2	26.5
Fe	19.0	48.8	9.5	13.8	7.4
Ni	-	1.2	1.2	2.8	2.8
O	60.3	50.0	63.1	61.2	63.2

As expected, the presence of Fe and Ni was verified for the bNP/CHI_(susp.) systems. The presence of carbon was also verified for the different samples. The occurrence of oxygen in the samples is due to the presence of chitosan and iron oxides/hydroxides. This study conducted using the EDS technique revealed the following Ni:Fe weight ratios: 0.02:0.98, 0.17:0.83, and 0.27:0.73. Thus, the different metallic nanoparticles were described in the present study as 2-bNP/CHI_(susp.), 17-bNP/CHI_(susp.), and 27-bNP/CHI_(susp.), respectively.

The XRD data are presented in Figure 6. The first aspect to be noted is the predominant amorphous character of the diffractograms, showing broad background signals.

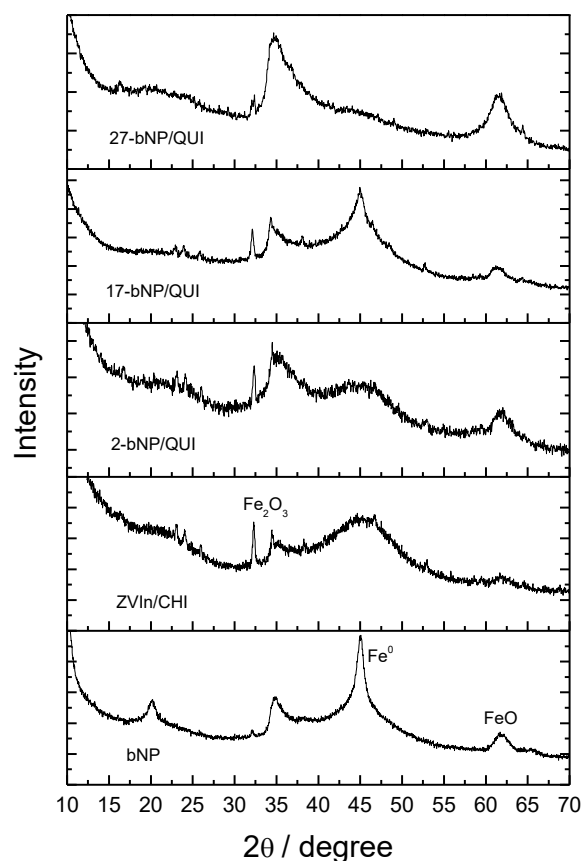


Figure 6. Diffractograms obtained for the different metallic systems composed of nanoparticles.

With the exception of the 27-bNP/CHI_(susp.) system, the diffractograms showed a band centred at $\sim 45^\circ$. Similar findings were recently reported by Weng *et al.*²³ and by Kuang *et al.*²⁵. In fact, the most intense peak of Fe⁰ is expected at 44.7° (ICSD 631728). On the whole, these findings are consistent with the presence of Fe⁰ as small clusters with poor crystallinity.

Additional interesting findings were verified in the diffractograms for the 30–40° and 60–65° intervals, where the XRD bands can be attributed to the presence of $\text{Na}_3\text{Fe}_5\text{O}_9$ and non-stoichiometric Fe^{3+} oxide-hydroxide, as well as FeO . It is worth mentioning that the presence of anhydrous or hydrated iron oxide-hydroxide for as-synthesised metallic nanoparticles was recently reported by different authors^{22, 26, 27}.

The specific surface area (SSA) and pore size distribution (PSD) were obtained for the 17-bNP/CHI_(susp.) system from the BET and BJH analyses, respectively (see [Supplementary Material, Fig. S1](#)). An SSA value of 769 $\text{m}^2 \text{g}^{-1}$ was verified for the 17-bNP/CHI_(susp.) system. On the contrary, an SSA value of only 33 $\text{m}^2 \text{g}^{-1}$ was verified for the 17-bNP system (see [Supplementary Material, Fig. S1](#)). Lin *et al.*²⁸ reported an SSA value of 15 $\text{m}^2 \text{g}^{-1}$ for the non-stabilised Fe^0 - Ni^0 nanoparticles. In addition, Weng *et al.*²³ reported an SSA value of 85.6 $\text{m}^2 \text{g}^{-1}$ for the chitosan-stabilised nanoparticles containing Fe^0 and Ni^0 . A comparison of these findings with those obtained in the present work highlights the higher SSA-value obtained for the 17-bNP/CHI_(susp.) system.

The high specific surface area obtained for 17-bNP/CHI_(susp.) can be ascribed to a good dispersion of the Fe^0 - Ni^0 nanoparticles propitiated by the stabilising agent (e.g., CHI) since the latter strongly inhibits the agglomeration phenomenon. It is worth mentioning that the high SSA-value obtained for the 17-bNP/CHI_(susp.) system can improve the removal rate of NMS. Also, it was verified a narrow interval for the PSD (e.g., 17–21 nm) for this particular system, characterising the existence of mesopores.

The 17-bNP/CHI_(susp.) system was also characterised using the Mössbauer technique (see [Supplementary Material, Fig. S2](#)). The experimental findings were simulated using a distribution function associated with super-paramagnetic particles containing Fe. The band (e.g., doublet distribution) was characterised by isomeric shifts in the range of 0.137 to 0.146 mm s^{-1} . Also, it was verified a quadrupole splitting in the range of 0.0 to 2.0 mm s^{-1} . However, the most probable value is 0.7 mm s^{-1} . In the Mössbauer spectrum, the super-paramagnetic behaviour appears as doublet signals. This relatively broad distribution of quadrupole confirms the presence of iron phases exhibiting a poor degree of crystallinity (e.g., oxide-hydroxides and $\alpha\text{-Fe}_2\text{O}_3$), as was

previously verified in the XRD study. These findings are in good agreement with the literature^{29–33}.

3.5 Nimesulide removal with the 17-bNP/CHI system

UV-Vis spectra obtained as a function of the reductive degradation reaction are presented in [Figure 7](#).

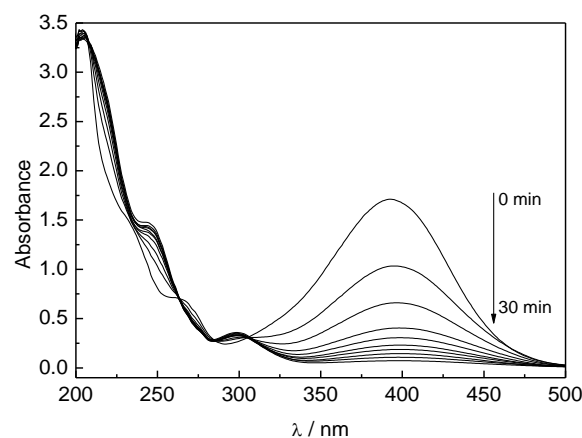


Figure 7. UV-Vis spectra of the dissolved organic matter obtained as a function of the reaction time. Conditions: $[\text{NMS}]_0 = 40 \text{ mg L}^{-1}$; $[\text{17-bNP/CHI}]_0 = 0.8 \text{ g L}^{-1}$; $T = 24 \pm 3 \text{ }^\circ\text{C}$.

It is clearly verified that the UV-band centred at 393 nm ($t = 0$) strongly decreased exhibiting a small bathochromic shift as the reductive degradation reaction proceeds. In principle, these findings are related to the reduction of the nitroaromatic moiety present in the molecular structure of NMS⁹. In addition, the appearance of a new band in the 230–330 nm interval of the spectrum can be attributed to the formation of an aromatic by-product. According to the literature⁵, the initial step in the redox reaction involving the NACs and Fe^0 -based nanoparticles is the hydrogenation of the N–O bond resulting in the appearance of nitroso compounds which can be then hydrogenated with the formation of hydroxylamine compounds. Finally, these compounds can be converted in other substances (e.g., NH_4^+ and/or N_2).

According to the literature³⁴, the agglomerates containing the bimetallic nanoparticles partially covered by an insulating oxide layer may result in the water splitting with the generation of hydroxyl radicals. As a result, the organic substance (NMS)

might also be degraded by an advanced oxidation process. However, this possibility was not considered in this study since the total organic carbon (TOC) did not change over the course of the redox reaction with NMS.

The chromatography analysis (HPLC) was carried out for different reaction times (see [Supplementary Material, Fig. S3](#)). It was verified a strong reduction of the peak exhibited by NMS (e.g., elution at ~ 11 min). In addition, the occurrence of a less intense peak observed at an elution time of 5.3 min can be ascribed to the formation of an aromatic substance. These findings are in good agreement with the UV-Vis study (see [Figure 7](#) and the discussion thereof).

3.6 Influence of the nanoparticle concentration on the reductive degradation of NMS

[Figure 8](#) shows the degradation of NMS in terms of the removal efficiency as a function of the nanoparticle concentration using the 17-bNP/CHI_(susp.) system. [Table 2](#) gathers the values of the apparent heterogeneous rate constant (k_{ap}) obtained for the reductive degradation of NMS.

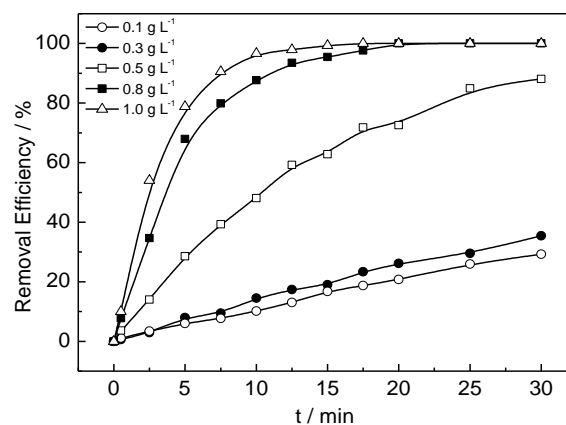


Figure 8. Removal efficiency as a function of the 17-bNP/CHI concentration. Conditions: $[NMS]_0 = 40$ mg L⁻¹, $f = 250$ rpm; $T = 24 \pm 3$ °C.

As can be seen, for an increase in the concentration of nanoparticles from 0.1 to 1.0 g L⁻¹ the degradation increased from 18 % to 100 % ($\Delta t = 15$ min), respectively. As a result, k_{ap} -values (see [Table 2](#)) increased from 1.17×10^{-2} to 3.29×10^{-2} min⁻¹, respectively.

Table 2. The kinetic parameter (k_{ap}) obtained for the different concentrations of the bimetallic nanoparticles

$[17\text{-bNP/CHI}]_0$ (g L ⁻¹)	k_{ap} (min ⁻¹)	r^2
0.1	1.17×10^{-2}	0.995
0.3	1.45×10^{-2}	0.996
0.5	7.20×10^{-2}	0.992
0.8	2.14×10^{-2}	0.997
1.0	3.29×10^{-2}	0.996

Conditions: $[NMS]_0 = 40$ mg L⁻¹; $T = 24 \pm 3$ °C and $f = 250$ rpm.

3.7 The reuse of the bimetallic nanoparticles in different experimental runs

It was verified after the first application of the nanoparticles in the reductive treatment that their reuse and stability (dispersability) strongly depend on $[NMS]_0$. In fact, it was verified that when $[NMS]_0 < 30$ mg L⁻¹ and $[17\text{-bNP/CHI}_{(susp.)}]_0 = 1.0$ g L⁻¹ the bimetallic nanoparticles might be only reused twice with a loss in efficacy, i.e., the use of the non-fresh nanoparticles in a second experimental run resulted in a decreased removal of about 30–50 %. In addition, it was confirmed that when $[NMS]_0 > 30$ mg L⁻¹ and $[17\text{-bNP/CHI}_{(susp.)}]_0 = 1.0$ g L⁻¹ the bimetallic

nanoparticles can no longer be used for promoting the degradation of NMS in a second experimental run. In fact, during a second experiment using the same bimetallic nanoparticles, these species were completely oxidised with the formation of a brownish precipitate that exhibited characteristics of the hydrated iron oxide. In this sense, the brownish precipitate was dried under vacuum and then subjected to the EDS analysis where the presence of iron, oxygen, and a low content of carbon were confirmed.

Grieger *et al.*³⁵ conducted a study on the environmental benefits and risks involving the use of Fe⁰-based nanoparticles in remediation processes. It was verified by these authors that

there are no significant risks to the environment in these cases. In fact, the solid product (e.g., mostly oxides) obtained after the reductive degradation of organic substances is not soluble in water and its presence in the environment does not pose any hazard.

3.8 Dependence of the heterogeneous rate constant on the initial concentration of nimesulide

Table 3 shows the k_{ap} -values obtained for the different concentrations of nimesulide.

Table 3. The kinetic parameter (k_{ap}) obtained for the different concentrations of nimesulide

[NMS] ₀ (mg L ⁻¹)	k_{ap} (min ⁻¹)	r^2
10	1.85	0.991
20	1.74×10^{-1}	0.996
30	3.11×10^{-1}	0.996
40	2.14×10^{-1}	0.997
50	9.57×10^{-2}	0.997

Conditions: [17-bNP/CHI]₀ = 0.8 g L⁻¹; $T = 24 \pm 3$ °C and $f = 250$ rpm

As can be seen, k_{ap} -values strongly decreased from 1.85 min⁻¹ to 9.57×10^{-2} min⁻¹ for an increase in the concentration of nimesulide from 10 to 50 mg L⁻¹, respectively. This behaviour indicates the occurrence of a surface heterogeneous redox reaction where there is a competition between the adsorbates (e.g., NMS) for the active Fe⁰-sites and, therefore, the overall concentration of the active surface sites available for the reductive degradation reaction can considerably decrease with an increase of the nimesulide concentration.

For the special case when [NMS]₀ = 10 mg L⁻¹, it was verified a removal percentage of 100 % for NMS after 2.5 min of reaction. Nonetheless, in the case of higher [NMS]₀-values a removal percentage higher than 75 % was only obtained after 15 min of reaction. These findings are in agreement with the literature²².

3.9 FT-IR analysis of the 17-bNP/CHI system

The FT-IR study was carried out under different experimental conditions for CHI_(s) and 17-bNP/CHI_(susp.) (see [Supplementary Material, Figure S4](#)). First, it was observed that the major absorption bands exhibited by CHI were also verified for the 17-bNP/CHI_(susp.) system, before and after the reductive reaction, thus confirming the presence of

CHI in the bimetallic nanoparticle system. The strong absorption band located at 3268 cm⁻¹, observed for the stabilised nanoparticles, can be ascribed to the presence of water, as well as to the symmetric stretching of the N–H bond of the amide groups of CHI^{23, 36}. The band observed at 1643 cm⁻¹ can be ascribed to the symmetric stretching of the N–H bond. The other bands observed at 1373 and 1052 cm⁻¹ are related to bending of the C–CH₃ bond and the symmetric stretching of the C–O bond, respectively^{23, 36}. On the whole, the FT-IR findings indicate that the chemical properties of CHI are almost unaffected by the reductive degradation reaction.

3.10 Identification of the by-product formed during the reductive degradation of nimesulide

The LC-ESI-MS analysis was accomplished for the by-product obtained at the elution time of 5.3 min. [Figure 9](#) shows the spectra obtained for the NMS (A) and by-product (B) after the redox reaction with the 17-bNP/CHI_(susp.) system. As can be seen, the nimesulide is identified by the positive ion [M + H]⁺ exhibiting an m/z ratio of 309 Da, while the by-product obtained from the catalytic hydrogenation of NMS is identified by an m/z ratio of 247 Da.

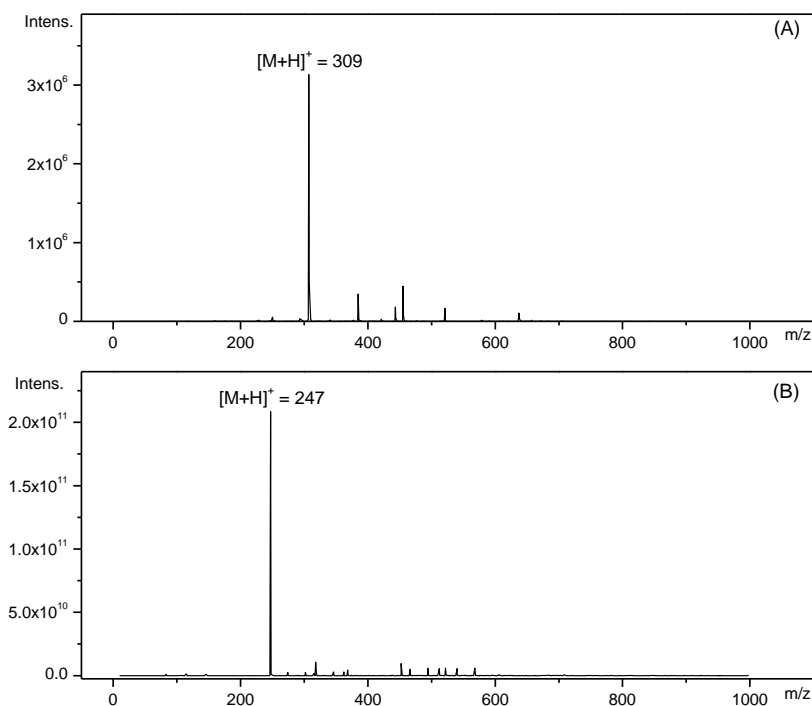


Figure 9. ESI-MS spectra obtained before (A) and after (B) the reductive reaction of NMS with 17-bNP/CHI. Conditions: $[\text{NMS}]_0 = 40 \text{ mg L}^{-1}$ and $[\text{17-bNP/CHI}]_0 = 0.8 \text{ g L}^{-1}$.

Taking into account the literature⁶, it was proposed in the present study that the bimetallic nanoparticles composed of 17-bNP/CHI_(susp.) resulted in the formation of adsorbed H[•]-radicals due to the catalytic action of the Ni⁰-centres.

Afterward, these radicals were incorporated in the molecular structure of NMS resulting in the reductive degradation/conversion of the parental substance. The overall redox process is shown in Figure 10.

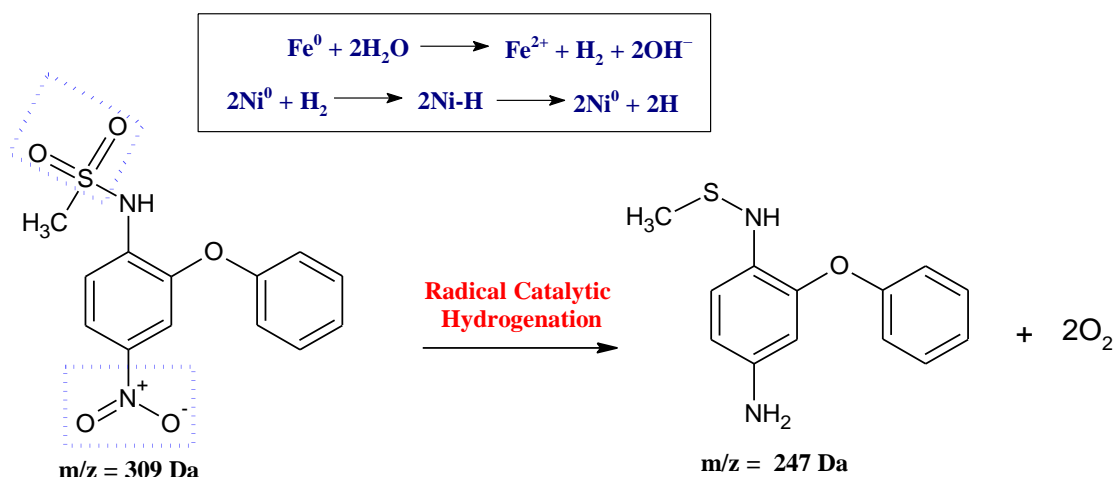


Figure 10. Representation of the reductive transformation of the parental substance (NMS) during the redox reaction with the bimetallic nanoparticles composed of 17-bNP/CHI.

As can be seen, the redox process is characterised by the formation of hydrogen from the water splitting in conjunction with the

oxidation of the Fe⁰-sites. Afterward, the hydrogen molecule is converted into hydrogen radicals due to the catalytic action of Ni⁰. As a result, the

degradation/transformation of NMS is propitiated by its reaction with the hydrogen radicals with the concomitant release of two oxygen molecules. In this sense, the removal of the nitro and sulphonyl groups during the redox process resulted in the formation of an amine and thioester by-product characterised by an m/z ratio of 247 Da.

From the above considerations, it can be expected the formation of less-harmful organic substances after the reductive treatment since the functional groups present in the structure of NMS were removed/converted during the redox reaction⁹. Therefore, the use of bimetallic nanoparticles containing Fe and Ni stabilised with chitosan in reductive treatment processes aiming for the degradation of NACs, as is the case of nimesulide, may be quite interesting from the environmental viewpoint.

4. Conclusions

The suspension containing the chitosan (CHI)-stabilized Ni⁰-Fe⁰ nanoparticles denoted as bNP/CHI_(susp.) is very active for promoting the removal/transformation of nimesulide present in water. The stabilising agent (CHI) prevented the agglomeration phenomenon thus strongly increasing the redox activity of the bimetallic nanoparticles for the reductive degradation of nimesulide. It was verified that the best composition of the bimetallic system contains 17 wt.% Ni and 83 wt.% Fe (e.g., 17-bNP/CHI_(susp.)). The XRD and Mössbauer analyses revealed the predominance of amorphous structures for iron-rich phases containing Fe⁰ and Fe₂O₃.

The presence of the catalyst (Ni⁰) is essential for promoting the reductive degradation of nimesulide where the functional groups of this substance are converted/modified by incorporation of the hydrogen radicals formed during the oxidation of the Fe⁰-centres.

The analysis of the by-product formed during the redox reaction revealed the formation of a substance containing the amine and thioester functionalities. In this sense, the present study suggests that the reductive removal/transformation of nimesulide using the 17-bNP/CHI_(susp.) system can be useful for the reduction of the toxicity intrinsic to this kind of NAC substance.

5. Acknowledgements

L. M. Da Silva wishes to thank the “*Conselho Nacional de Desenvolvimento Científico e Tecnológico* – CNPq” (PQ-2 grant) and “*Fundação de Ampara à Pesquisa do Estado de Minas Gerais* – FAPEMIG” (APQ-02739-17).

6. References

- [1] Campanha, M.B., Awan, A.T., de Sousa, D.N.R. Grosseli, G. M.; Mozeto, A. A.; Fadini, P.S. *Environ. Sci. Pollut. Res.* 22 (2015) 7936-7947. <https://doi.org/10.1007/s11356-014-3929-x>.
- [2] Silveira, M.A.K., Caldas, S.S., Guilherme, J.R., Costa, F.P., Guimarães, B.S., Cerqueira, M.B.R. et al., Quantification of Pharmaceuticals and Personal Care Product Residues in Surface and Drinking Water Samples by SPE and LC-ESI-MS/MS, *J. Braz. Chem. Soc.* 24 (2013) 1385–1395. <https://doi.org/10.5935/0103-5053.20130176>.
- [3] Papageorgiou, M., Kosma, C., Lambropoulou, D., Seasonal occurrence, removal, mass loading and environmental risk assessment of 55 pharmaceuticals and personal care products in a municipal wastewater treatment plant in Central Greece, *Sci. Total Environ.* 543 (2016) 547–569. <https://doi.org/10.1016/j.scitotenv.2015.11.047>.
- [4] Crane, R.A., Scott, T.B., Nanoscale zero-valent iron: future prospects for an emerging water treatment technology, *J. Hazard. Mater.* 211 (2012) 112–125. <https://doi.org/10.1016/j.jhazmat.2011.11.073>.
- [5] Liu, W.-J., Qian, T.-T., Jiang, H., Bimetallic Fe nanoparticles: Recent advances in synthesis and application in catalytic elimination of environmental pollutants, *Chem. Eng. J.* 236 (2014) 448–463. <https://doi.org/10.1016/j.cej.2013.10.062>.
- [6] Gao, Y., Wang, F., Wu, Y., Naidu, R., Chen, Z., Comparison of degradation mechanisms of microcystin-LR using nanoscale zero-valent iron (nZVI) and bimetallic Fe/Ni and Fe/Pd nanoparticles, *Chem. Eng. J.* 285 (2016) 459–466. <https://doi.org/10.1016/j.cej.2015.09.078>.
- [7] Lima, A.B., Chaves, S.C., Da Silva, L.M., Pereira, P.F., Richter, E.M., Santos, W.T.P.,

- Determinação de nimesulida por análise por injeção em fluxo com detecção amperométrica de múltiplos pulsos, *Quim. Nova* 39 (2013) 1296–1302. <https://doi.org/10.1590/S0100-40422013000900004>.
- [8] Bernareggi, A., Clinical pharmacokinetics and metabolism of nimesulide, *Inflammopharmacology* 9 (2001) 81–89. <https://doi.org/10.1163/156856001300248353>.
- [9] Agrawal, A., Tratnyek, P., Reduction of nitro aromatic compounds by zero-valent iron metal, *Environ. Sci. Technol.* 30 (1995) 153–160. <https://doi.org/10.1021/es950211h>.
- [10] Fu, F.; Dionysios, D.D.; Liu, H., The use of zero-valent iron for groundwater remediation and wastewater treatment: A review, *J. Hazard. Mater.* 267 (2014) 194–200. <https://doi.org/10.1016/j.jhazmat.2013.12.062>.
- [11] Kustov, L.M.; Finashina, E.D.; Shuvalova, E.V.; Tkachenko, O.P.; Kirichenko, O.A., Pd–Fe nanoparticles stabilized by chitosan derivatives for perchloroethene dechlorination, *Environ. Int.* 37 (2011) 1044–1052. <https://doi.org/10.1016/j.envint.2011.05.003>.
- [12] Cai, Z.; Fu, J.; Du, P.; Zhao, X.; Hao, X.; Liu, W.; Zhao, D., Reduction of nitrobenzene in aqueous and soil phases using carboxymethyl cellulose stabilized zero-valent iron nanoparticles, *Chem. Eng. J.* 332 (2018) 227–236. <https://doi.org/10.1016/j.cej.2017.09.06>.
- [13] Fang, Z., Chen, J., Qiu, X., Qiu, X., Cheng, W., Zhu, L., Effective removal of antibiotic metronidazole from water by nanoscale zero-valent iron particles, *Desalination* 268 (2011) 60–67. <https://doi.org/10.1016/j.desal.2010.09.051>.
- [14] Franco, D.V., Da Silva, L.M., Jardim, W.F., Reduction of hexavalent chromium in soil and ground water using zero-valent iron under batch and semi-batch conditions, *Water Air Soil Poll.* 197 (2009) 49–60. <https://doi.org/10.1007/s11270-008-9790-0>.
- [15] Franco, D.V., Da Silva, L.M., Jardim, W.F., Chemical reduction of hexavalent chromium and its immobilisation under batch conditions using a slurry reactor, *Water Air Soil Poll.* 203 (2009) 305–315. <https://doi.org/10.1007/s11270-009-0013-0>.
- [16] Cao, J., Xu, R., Tang, H., Tang, S., Cao, M., Synthesis of monodispersed CMC-stabilized Fe-Cu bimetal nanoparticles for in situ reductive dechlorination of 1,2,4-trichlorobenzene, *Sci. Total Environ.* 409 (2011) 2336–2341. <https://doi.org/10.1016/j.jece.2016.09.038>.
- [17] Wang, D.R.Y., Zhou, J., Liu, L., Huang, C.J., Zhou, D., Fu, L., Characterization and toxicology evaluation of chitosan nanoparticles on the embryonic development of zebra fish, *Carbohydr. Polym.* 141 (2016) 204–210. <https://doi.org/10.1016/j.carbpol.2016.01.012>.
- [18] Liu, T., Zhao, L., Sun, D., Tan, X., Entrapment of nanoscale zero-valent iron in chitosan beds for hexavalent chromium removal from wastewater, *J. Hazard. Mat.* 184 (2012) 724–730. <https://doi.org/10.1016/j.jhazmat.2010.08.099>.
- [19] Ruela, A.L.M., Araújo, M.B., Pereira, G.R., Desenvolvimento e validação de um método analítico rápido por cromatografia líquida de alta eficiência para determinação de nimesulida em estudos de liberação in vitro, *Quim. Nova* 32 (2009) 165–168. <https://doi.org/10.1590/S0100-40422009000100031>.
- [20] Lin, Y.-T., Weng, C.-H., Chen, F.-Y., Effective removal of AB24 dye by nano/micro-size zero-valent iron, *Sep. Purif. Technol.* 64 (2008) 26–30. <https://doi.org/10.1016/j.seppur.2008.08.012>.
- [21] Han, Y., Li, W., Zhang, M., Tao, K., Catalytic dechlorination of monochlorobenzene with a new type of nanoscale Ni(B)/Fe(B) bimetallic catalytic reductant, *Chemosphere* 72 (2008) 53–58. <https://doi.org/10.1016/j.chemosphere.2008.02.002>.
- [22] Chen, Z.X., Jin, X.Y., Chen, Z., Megharaj, M., Naidu, R., Removal of methyl orange from aqueous solution using bentonite-supported nanoscale zero-valent iron, *J. Colloid Interface Sci.* 363 (2011) 601–607. <https://doi.org/10.1016/j.jcis.2011.07.057>.
- [23] Weng, X., Lin, S., Zhong, Y., Chen, Z., Chitosan stabilized bimetallic Fe/Ni nanoparticles

- used to remove mixed contaminants-amoxicillin and Cd(II) from aqueous solutions, *Chem. Eng. J.* 229 (2013) 27–34. <https://doi.org/10.1016/j.cej.2013.05.096>.
- [24] Segura, Y., Martínez, F., Melero, J.A., Fierro, J.L.G., Zero valent iron (ZVI) mediated Fenton degradation of industrial wastewater: Treatment performance and characterization of final Composites, *Chem. Eng. J.* 269 (2015) 298–305. <https://doi.org/10.1016/j.cej.2015.01.102>.
- [25] Kuang, Y.; Du, J.; Zhou, R.; Chen, Z.; Megharaj, M.; Naidu, R., Calcium alginate encapsulated Ni/Fe nanoparticles beads for simultaneous removal of Cu (II) and monochlorobenzene, *J. Colloid Interface Sci.* 447 (2015) 85–91. <https://doi.org/10.1016/j.jcis.2015.01.080>.
- [26] Liu, X.; Chen, Z.; Chen, Z.; Megharaj, M.; Naidu, R., Remediation of Direct Black G in wastewater using kaolin-supported bimetallic Fe/Ni nanoparticles, *Chem. Eng. J.* 223 (2013) 764–771. <https://doi.org/10.1016/j.cej.2013.03.002>.
- [27] Liu, Z.; Gu, C.; Ye, M.; Bian, Y.; Cheng, Y.; Wang, F.; Yang, X.; Yang, S.; Jiang, X., Debromination of polybrominated diphenyl ethers by attapulgite-supported Fe/Ni bimetallic nanoparticles: Influencing factors, kinetics and mechanism, *J. Hazard. Mater.* 298 (2015) 328–337. <https://doi.org/10.1016/j.jhazmat.2015.05.032>.
- [28] Lin, C., Shih, Y., MacFarlane, J., Amphiphilic compounds enhance the dechlorination of pentachlorophenol with Ni/Fe bimetallic nanoparticles, *Chem. Eng. J.* 262 (2015) 59–67. <https://doi.org/10.1016/j.cej.2014.09.038>.
- [29] Marchal, G., Mangin, P., Piecuch, M., Janot, C., Mössbauer study of magnetic ordering in amorphous Fe-Si alloys, *J. Physique Colloq.* 37 (1976) C6-763-768. <https://doi.org/10.1051/jphyscol:19766160>.
- [30] Tartaj, P., González-Carreño, T., Bomati-Miguel, O., Serna, C.J., Bonville, P., Magnetic behaviour of superparamagnetic Fe nanocrystals confined inside submicron-sized spherical silica particles, *Phys. Rev. B* 69 (2004) 094401-1-094401-8. <https://doi.org/10.1103/PhysRevB.69.094401>.
- [31] Murad, E., Mössbauer spectroscopy of clays, soils and their mineral constituents, *Clay Minerals* 45 (2010) 413–430. <https://doi.org/10.1180/claymin.2010.045.4.413>.
- [32] van der Kraan, A. M., Mössbauer effect studies of surface ions of ultrafine α -Fe₂O₃ particles, *Phys. Status Solidi A* 18 (1973) 215–226. <https://doi.org/10.1002/pssa.2210180120>.
- [33] Zboril, R., Mashlan, M., Petridis, D., Iron (III) Oxides from Thermal Processes Synthesis, Structural and Magnetic Properties, Mössbauer Spectroscopy Characterization, and Applications, *Chem. Mater.* 14 (2002) 969–982. <https://doi.org/10.1021/cm0111074>.
- [34] Bokare, A.D., Chikate, R.C., Rode, C.V., Paknikar, K.M., Effect of surface chemistry of Fe–Ni nanoparticles on mechanistic pathways of azo dye degradation, *Environ. Sci. Technol.* 41 (2007) 7437–7443. <https://doi.org/10.1021/es071107q>.
- [35] Grieger, K.D.; Fjordbøge A.; Hartmann, N.B.; Eriksson, E.; Bjerg, P.L.; Baun, A., Environmental benefits and risks of zero-valent iron nanoparticles (nZVI) for in situ remediation: Risk mitigation or trade-off? *Journal of Contaminant Hydrology* 118 (2010) 165–183. <https://doi.org/10.1016/j.jconhyd.2010.07.011>.
- [36] Geng, B., Jin, Z., Li, T., Qi, X., Preparation of chitosan-stabilized Fe(0) nanoparticles for removal of hexavalent chromium in water, *Sci. Total Environ.* 407 (2009) 4994–5000. <https://doi.org/10.1016/j.scitotenv.2009.05.051>.

Supplementary Material

Synthesis of chitosan-stabilised iron and nickel nanoparticles and the application in the reductive degradation of nimesulide

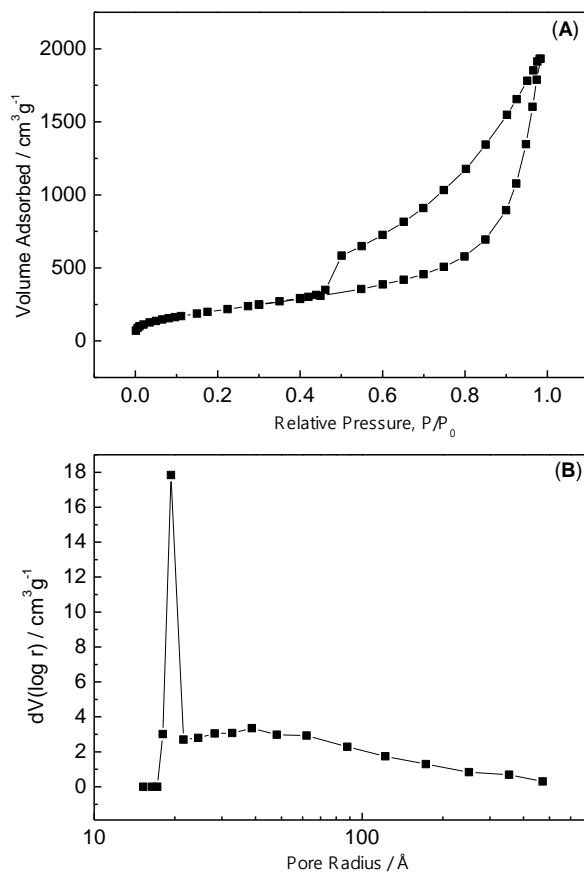


Figure S1. BET analysis: (A) isotherm plot and (B) pore radius distribution obtained for 17-bNP/CHI.

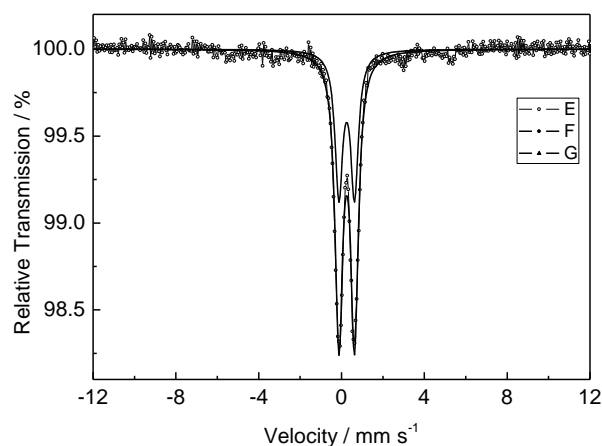


Figure S2. ^{57}Fe Mössbauer spectrum obtained for the 17-bNP/CHI sample at room temperature. The fitted curve is the sum of two signal distributions also shown (displaced on the vertical scale for clarity).

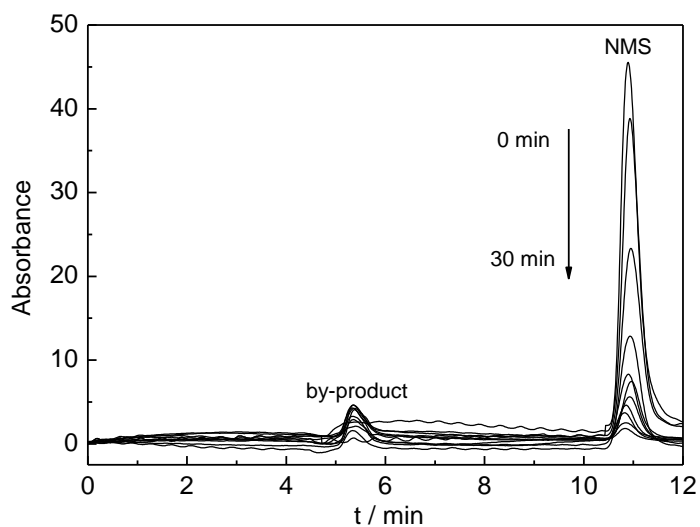


Figure S3. HPLC chromatograms obtained for the treated samples as a function of the reaction time. Conditions: $[\text{NMS}]_0 = 40 \text{ mg L}^{-1}$; $[\text{17-bNP/CHI}]_0 = 0.8 \text{ g L}^{-1}$; $T = 24 \pm 3 \text{ }^\circ\text{C}$.

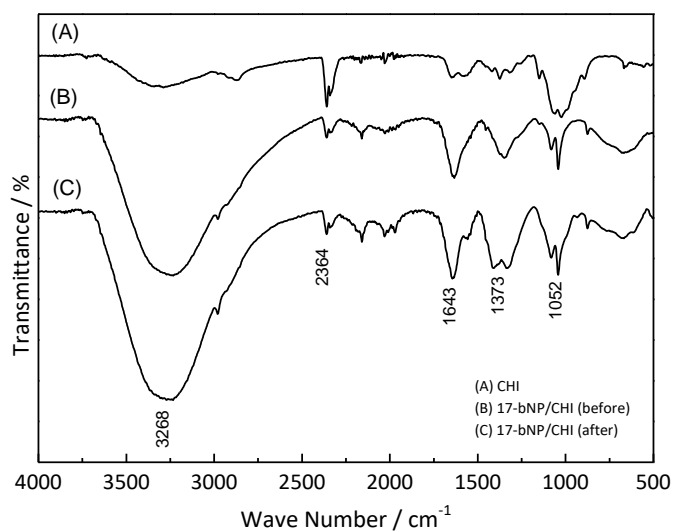


Figure S4. FT-IR spectra obtained for pure CHI and for 17-bNP/CHI, before and after the reductive reaction with NMS.